Inpainting Images on Implicit Surfaces

Chunlin Wu Jiansong Deng Wenming Zhu
Falai Chen
Department of Mathematics
University of Science and Technology of China
Hefei, Anhui, 230026
China

Abstract

Planar image processing has been widely investigated for many years. The processing operations include denoising, edge enhancement, edge detecting, inpainting, and others. But there exists little work about processing images on surfaces, since it is difficult to extend the classic methods to deal with the problem. In this paper, we study the inpainting algorithm of images on implicit surfaces based on the method of energy minimizing and PDE. It's a generalization of the inpainting algorithm of planar images. An intrinsic energy functional is defined over surfaces. Energy minimization problem is solved by a numerical method, which needs data extrapolating. Another contribution of this paper is a theorem on how to control data extrapolating for processing images on implicit surfaces. The experiment results show the efficiency of our method.

Keywords: Image processing, implicit surfaces, inpainting, energy functionals.

1 Introduction

Planar image processing has been investigated for many years, and the typical processing operations include denoising, edge enhancement, edge detecting, inpainting. Among them, inpainting is an artistic synonym for image interpolation. It makes use of computers to repair distorted images automatically like artists. Usually the distortion of images includes scratches, block missing, etc. Image inpainting algorithms can be applied to not only information recovery, but also removal of texts and absonant objectives on photos. Currently there are many inpainting algorithms for planar images. They are mostly based on variation and PDE. Excellent results are obtained by these algorithms.

Based on the anisotropic diffusion model [1] proposed by P. Perona and J. Malik, and the energy minimizing variation model [2] by S. Osher, the application of variational principle and PDE to image processing becomes more and more comprehensive, including image denoising, image deblurring, image inpainting, edge enhancing and detecting, and image decomposition. Usually there are two kinds of image data: gray image and color image (vector-value image). Through variational method and PDE, researchers proposed many edge preserving denoising algorithms for gray images [1, 2, 3, 4, 5, 6]. Furthermore, denoising models and algorithms for color images also appear [7].

Image inpainting problem was first introduced by M. Bertalmio *et al* [8] when they developed their first PDE based model. Afterward T.F. Chan and J. Shen proposed many efficient models based on variational principle and PDEs [9, 10, 11, 12, 13, 14, 15]. These models include local inpainting algorithm [9] which is fastest but can only handle smooth images, TV inpainting algorithm [13] which can handle not only smooth images but also discontinuous images

for its edge preserving property, and inpainting algorithms based on Euler's elastica energy [10, 11]. Image inpainting from multiple views images was first introduced in [12]. In [15] S. Esedoglu and J. Shen proposed an inpainting algorithm based on Mumford-Shah-Euler energy minimization. For this MSE model, T.F. Chan gave a fast numerical method based on Level Set Method[19]. Video inpainting was first studied by M. Bertalmio through Navier-Stokes equation in [16], then J. Shen proposed an inpainting model based on BV (Bounded Variation) image model and Bayes statistical theory in [18]. In [17] J. Shen gave a general summation of image processing based on variational principle and PDEs. Inpainting algorithms for planar images work very well now, but video inpainting[16, 18] is still a large problem.

All of these works process classical images, that is, planar images. In computer graphics, sometimes we will face images on surfaces, such as textures on surfaces. G. Sapiro and S. Osher proposed a framework of processing of signals on implicit surfaces [20]. Based on this framework, they studied Harmonic Maps energy of images on surfaces. Through variational method, the authors obtained corresponding PDEs. They used these PDEs to denoise images on implicit surfaces. It's a generalization from planar images to images on implicit surfaces. In this paper, we generalize inpainting algorithm for planar images to that for images on implicit surfaces. We favor the generalization of the TV inpainting algorithm for robustness and computational efficiency. In fact, all images that can be repaired by local inpainting can also be repaired by TV inpainting, that is, TV inpainting can handle more kinds of image data then local inpainting. On the other hand, models based on Euler's elastica energy result in high order PDEs, and numerical methods for these high order PDEs are too complex and not very efficient.

In next section, we review some inpainting models for planar images. The inpainting model for images on implicit surfaces will be introduced in section 3. In section 4, the inpainting algorithm and steps with some examples are given. Finally, we will conclude the paper in section 5.

2 Inpainting Models for Planar Images

Planar image processing problems include image denoising, deblurring, edge enhancement, detection, and so on. Image decomposition and image inpainting appeared recently as a hot research direction. After development of several decades, there are many classical methods, such as Fourier analysis and wavelet analysis, proposed for these operations. In this paper, we consider processers based on variational principle and PDEs. To construct this type of processers, an energy functional should be defined first. Then, we minimize this functional, and obtain an Euler-Lagrange equation via variational method. Finally, the Euler-Lagrange equation is solved by well developed numerical methods for the corresponding PDE. It is the key part of this method that an energy functional should be defined in a reasonable way. For inpainting of planar images, there are a set of good works currently. Please refer to [8] by M. Bertalmio and G. Sapiro, and [9, 10, 11, 12, 13, 14, 15] by T.F. Chan, and so on, for details. In the following we review the models based on Harmonic Maps energy proposed by T.F. Chan, *et al.*

Consider a planar image f defined in domain $\Omega \subset \mathbb{R}^2$, usually a rectangle domain. $D \subset \Omega$ is a subregion in Ω, as shown in Fig. 1. We assume the part of f on D is distorted. To inpaint missing image data on D,

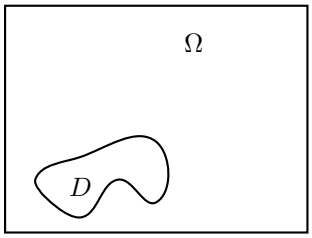

Figure 1: A planar domain Ω and $D \subset \Omega$

T.F. Chan proposed the following inpainting model (energy functional):

$$\min_u E[u, \Omega] = \int_\Omega |\nabla u|^p d\vec{x} + \lambda_D \frac{1}{2} \int_\Omega (f-u)^2 d\vec{x} \quad (1)$$

where

$$\lambda_D = \lambda \cdot 1_D = \lambda \cdot \begin{cases} 1, (x,y) \in \Omega \backslash D \\ 0, (x,y) \in D \end{cases}$$

Here function 1_D is called inpainting mask. T.F. Chan studied two cases: $p = 2$(local inpainting) and $p = 1$(TV inpainting). This energy minimization problem is solved by variational method and results in the corresponding Euler-Lagrange equation. T.F. Chan and J. Shen proposed two approaches to solve this equation. The first one is reformulating the equation into a developing equation by introducing a time variable and then solving it by difference schemes. The other method is based on iteration [4, 5].

3 Inpainting Images on Implicit Surfaces

In this section, we present our generalized inpainting model for images on implicit surfaces. Assume we have an implicit surface S as the zero level set of $\varphi : \mathbb{R}^3 \to \mathbb{R}$. $\varphi < 0$ at inside of S, and $\varphi > 0$ at outside of S. An image $f = f(x,y,z)|_S$ is observed. Observation is made by various instruments including human sensory such as human visual system. Usually observed data is noisy and the noise is considered to be a Gaussian. So the observed image f is not the true image. We assume the true image on S is $u = u(x,y,z)|_S$ and the information of u on $D \subset S$ is missing or distorted, as shown in Fig. 2. Now we want to recover u from observed f, especially repair the information on D (inpainting).

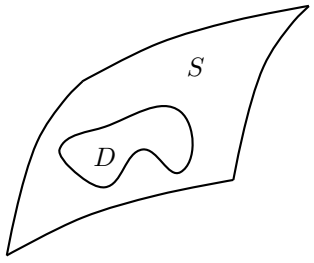

Figure 2: A surface S and $D \subset S$

Viewing this problem by vision phycology and Bayes statistics, the objective of inpainting is to obtain a maximum likelihood distribution, so that users accept it as the most possible "true data". That is, inpainting is to maximize the posterior probability $\text{Prob}(u|f,D)$ as follows (MAP):

$$\max_u \text{Prob}(u|f,D) = \frac{\text{Prob}(f|u,D) \cdot \text{Prob}(u)}{\text{Prob}(f,D)}. \quad (2)$$

To avoid the distribution construction from image data, we convert this Bayesian framework to energy minimization problem. Based on Gibbs-formula from statistical mechanics (the relation between probability and energy):

$$\text{Prob}(u) \propto \exp\left(-\beta E[u]\right),$$

it is easy to see maximizing $\text{Prob}(u|f,D)$ is just minimizing the corresponding energy

$$\min_u E_s[u|f,D] = E_s[f|u,D] + E_s[u] + \text{const}. \quad (3)$$

since f and D are given. In the following we will define the seemly energy functionals $E_s[f|u,D]$ and $E_s[u]$, which are the generalized form from planar images to images on implicit surfaces.

3.1 Energy Functionals on Implicit Surfaces

In this section energy functionals on implicit surfaces will be proposed first. Then through Dirac function, we relate these functionals to the Gibbs-formula.

These energy functionals are the generalized form of those used by T.F. Chan, *et al.* With the method of computing intrinsic gradient proposed by S. Osher in [20], we define Harmonic Maps energy functional on implicit surfaces. Let $\vec{v}$ be a vector in 3D space. Define an operator

$$P_{\vec{v}} := I - \frac{\vec{v} \otimes \vec{v}}{\|\vec{v}\|^2} \quad (4)$$

When $P_{\vec{v}}$ operates on a 3D vector, the operated vector is projected to the plane perpendicular to $\vec{v}$. So we can define

$$\nabla_S u := P_{\vec{N}} \nabla u \quad (5)$$

to be the intrinsic gradient of u to the surface S, where $\vec{N}$ is the normal vector of S. Then the Harmonic Maps energy functional of u on S is as follows:

$$E_s[u] = \int_S |\nabla_S u|^p dS \tag{6}$$

On the assumption of the Gaussian noise, we can define

$$E_s[f|u, D] = \lambda_D \frac{1}{2} \int_S (f-u)^2 dS, \tag{7}$$

where λ_D is similar to the case of planar images.

Integrating these two parts, we obtain an energy functional on implicit surface as follows

$$E_s[u|f, D] = \int_S |\nabla_S u|^p dS + \lambda_D \frac{1}{2} \int_S (f-u)^2 dS \tag{8}$$

Especially we call the functional Intrinsic Total Variation energy when $p = 1$.

Although this energy function is defined on surface S, we can convert it to the form in Euclidean space with help of Dirac function $\delta(\varphi)$. Concretely, we have

$$\begin{aligned} E_s[u|f, D] = &\int_{\Omega \subseteq \mathbb{R}^3} |P_{\nabla\varphi} \nabla u|^p \delta(\varphi) |\nabla\varphi| d\vec{x} \\ &+ \lambda_D \frac{1}{2} \int_{\Omega \subseteq \mathbb{R}^3} (f-u)^2 \delta(\varphi) |\nabla\varphi| d\vec{x} \end{aligned}$$

so according to Gibbs-formula, we obtain the inpainting model of images on implicit surfaces as follows

$$\min_u E_s[u|f, D] = \int_S |\nabla_S u|^p dS + \lambda_D \frac{1}{2} \int_S (f-u)^2 dS \tag{9}$$

Up to now, we have the energy functional of the inpainting model. By an projecting operator, we convert the gradient of u to the intrinsic gradient $\nabla_S u$, so our energy functional is intrinsic to the implicit surface S. Nevertheless, the gradient ∇u is still needed when numerical computing. However, we have only image data on the surface. Data extrapolating solves this problem perfectly. Before inpainting, we extrapolate the image data to a band $B \subset \mathbb{R}^3$ around S.

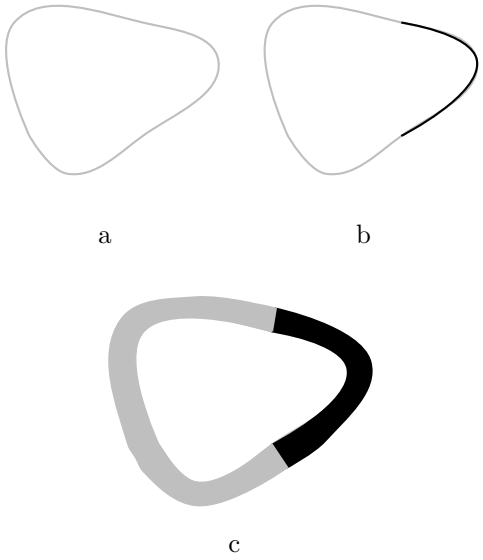

Figure 3: A curve and a function defined on it

3.2 Data Extrapolating

In this section our data extrapolating algorithm is given. The image data defined on implicit surface S is extrapolated to a band around S by this algorithm, which is based on a Hamilton equation proposed by S. Chen in [22] and applied to fluid dynamics originally. At first we show an example of curve for visuality. Assume we have a closed curve C as shown in Fig. 3(a). f is an image (a function essentially) defined on C. We show this image through the density information corresponding to it, as shown in Fig. 3(b). The extrapolated image data is showed in figure Fig. 3(c). We can see that the image data on C is now extrapolated to a band around C. In this band, the gradient of the image can be computed.

It is very natural that the extrapolated data had better keep constant along the normal direction of the level sets of φ, that is, $\nabla u \cdot \nabla\varphi = 0$. Here S is the zero level set of φ. Taking this into consideration, we extrapolate the data by a Hamilton equation as follows

$$u_t + \text{sign}(\varphi)(\nabla u \cdot \nabla\varphi) = 0, \tag{10}$$

where $\text{sign}(\varphi)$ is the sign function of φ.

This Hamilton equation is ill-posed for most function φ. When $t \to \infty$, the equation will not arrive a steady solution. Shocks will appear when t is large enough indeed. Fortunately we need only a narrow band to which the data is extrapolated, as shown in Fig. 3(c) for the case of curve. The band will be more and more wider as the solution time t grows up. So we solve the equation just in a short time. The following theorem describes the relationship between solution time t and the width of band.

Theorem 1 *Under the evolution of equation (10), function u will be extrapolated along the normal direction of the level sets of φ. At t, the function will be extrapolated to $X = \{(x,y,z) : \varphi(x,y,z) = \varphi_+^t(x,y,z)\}$(outside of S) and $Y = \{(x,y,z) : \varphi(x,y,z) = \varphi_-^t(x,y,z)\}$(inside of S), where*

$$\begin{aligned}\varphi_+^t(x,y,z) &= \int_0^t |\nabla\varphi(x_+(\tau), y_+(\tau), z_+(\tau))|^2 d\tau \\ \varphi_-^t(x,y,z) &= -\int_0^t |\nabla\varphi(x_-(\tau), y_-(\tau), z_-(\tau))|^2 d\tau\end{aligned} \tag{11}$$

Especially we have an estimation that u will be extrapolated to the level sets $\tilde{X} = \{(x,y,z) : \varphi(x,y,z) = \varphi_+^t\}$(outside of S) and $\tilde{Y} = \{(x,y,z) : \varphi(x,y,z) = \varphi_-^t\}$(inside of S) of φ, where

$$\begin{aligned}\varphi_+^t &= \min_{(x,y,z),\varphi(x,y,z)\geq 0} |\nabla\varphi|^2 t \\ \varphi_-^t &= -\min_{(x,y,z),\varphi(x,y,z)\leq 0} |\nabla\varphi|^2 t\end{aligned} \tag{12}$$

Proof: We just prove the case of the outside of S. The case of the inside is similar. According to the property of Hamilton-Jacobi equation, function u will be extrapolated along the normal direction of the level sets of φ under the revolution of equation (10) and the extrapolating velocity is

$$\begin{cases} \frac{dx}{dt} = \varphi_x \\ \frac{dy}{dt} = \varphi_y \\ \frac{dz}{dt} = \varphi_z \end{cases}$$

We assume that function u is extrapolated to $X = \{(x,y,z) : \varphi(x,y,z) = \varphi^t(x,y,z)\}$ at time t. According to the illation above, the information of u on a point (x_s, y_s, z_s) on S will march along a normal curve C_n from point (x_s, y_s, z_s). Here a "normal curve" is a curve like this: the starting point of the curve is on surface S (zero level set of φ) and the tangent vector is the normal vector of the level sets of φ anywhere along the curve. Suppose there is an object on a point on S. Let this object move with the velocity determined by equation (10), then it will move along the normal curve determined by the starting point. The object will arrive at a point of X at time t. It is obvious that any point (x,y,z) in X is on a certain normal curve whose starting point is $(x_s, y_s, z_s) \in S$ hypothetically. We have

$$\begin{cases} x = x(t) = \int_0^t \varphi_x d\tau + x_s \\ y = y(t) = \int_0^t \varphi_y d\tau + y_s \\ z = z(t) = \int_0^t \varphi_z d\tau + z_s \end{cases}$$

therefore,

$$\begin{aligned}&\varphi(x,y,z) = \varphi(x(t), y(t), z(t)) \\ =&\varphi\left(x_s + \int_0^t \varphi_x d\tau, y_s + \int_0^t \varphi_y d\tau, z_s + \int_0^t \varphi_z d\tau\right)\end{aligned}$$

It is obvious that the function above is a single variable function of t along any normal curve. Marking it renewedly

$$\varphi^t = \varphi(x,y,z) = \varphi(x(t), y(t), z(t))$$

Differentiating both sides, we obtain

$$\varphi_t^t = \varphi_x\varphi_x + \varphi_y\varphi_y + \varphi_z\varphi_z = \|\nabla\varphi(x(t), y(t), z(t))\|^2$$

Integrating the equation above and taking it into consideration that we extrapolate the data from the surface $S(\varphi = 0)$, the theorem is proved. Since

$$\begin{aligned}&\min_{(x,y,z),\varphi(x,y,z)\geq 0} |\nabla\varphi|^2 t \leq \varphi_+^t \leq \max_{(x,y,z),\varphi(x,y,z)\geq 0} |\nabla\varphi|^2 t \\ -&\max_{(x,y,z),\varphi(x,y,z)\leq 0} |\nabla\varphi|^2 t \leq \varphi_-^t \leq -\min_{(x,y,z),\varphi(x,y,z)\leq 0} |\nabla\varphi|^2 t\end{aligned}$$

equation (12) holds. ■

Because signed distance function is very important among presentations of implicit surfaces, we give the following corollary for this case.

Corollary 1 *If φ is the signed distance function of surface S, then u will be extrapolated along the normal direction of the level sets of φ under the revolution of equation (10). At t, u will be extrapolated to the level sets $\tilde{X} = \{(x,y,z) : \varphi(x,y,z) =$*

$\varphi_+^t\}$*(outside of* S*) and* $\tilde{Y} = \{(x,y,z) : \varphi(x,y,z) = \varphi_-^t\}$*(inside of* S*) of* φ*, where*

$$\varphi_+^t = t, \quad \varphi_-^t = -t \tag{13}$$

Proof: Since φ is the signed distance function of S, it follows that

$$|\nabla\varphi| \equiv 1$$

Substituting this into the theorem, our corollary is proved. ■

3.3 Euler-Lagrange Equation

According to the discussion above, we obtain a seemly energy functional. Simplifying the notation, our inpainting model is as follows:

$$\min_u E = \int_S |P_{\nabla\varphi}\nabla u|^p dS + \lambda_D \frac{1}{2}\int_S (f-u)^2 dS \tag{14}$$

In the section the corresponding Euler-Lagrange equation is given via variational method, and a method to solve this equation is presented.

Theorem 2 *(a)When the energy* E *is minimal, we have*

$$\frac{1}{|\nabla\varphi|}\nabla\cdot(p|P_{\nabla\varphi}\nabla u|^{p-2}P_{\nabla\varphi}\nabla u|\nabla\varphi|) + \lambda_D(f-u) = 0 \tag{15}$$

(b)Let

$$\frac{1}{|\nabla\varphi|}\nabla\cdot(p|P_{\nabla\varphi}\nabla u|^{p-2}P_{\nabla\varphi}\nabla u|\nabla\varphi|) + \lambda_D(f-u) = u_t, \tag{16}$$

then E *will decrease by the speed*

$$\frac{dE}{dt} = -\int_S (\frac{1}{|\nabla\varphi|}\nabla\cdot(p|P_{\nabla\varphi}\nabla u|^{p-2}P_{\nabla\varphi}\nabla u|\nabla\varphi|) + \lambda_D(f-u))^2 dS$$

as the solution time t *grows up.*

Proof: (a) In fact the corresponding Euler-Lagrange equation is needed. We import the Dirac function to obtain the variation of E and then give the Euler-Lagrange equation which minimizes the energy. Letting $\triangle E$ stand for the variation of E, we have

$$\begin{aligned}
\triangle E &= \int_S \triangle(|P_{\nabla\varphi}\nabla u|^p) dS + \lambda_D \frac{1}{2}\int_S \triangle((f-u)^2) dS \\
&= \int_{R^3} \triangle(|P_{\nabla\varphi}\nabla u|^p)\delta(\varphi)|\nabla\varphi| d\vec{x} \\
&\quad + \frac{\lambda_D}{2}\int_{R^3} \triangle((f-u)^2)\delta(\varphi)|\nabla\varphi| d\vec{x} \\
&= \int_{R^3} p|P_{\nabla\varphi}\nabla u|^{p-1} \triangle (|P_{\nabla\varphi}\nabla u|)\delta(\varphi)|\nabla\varphi| d\vec{x} \\
&\quad + \frac{\lambda_D}{2}\int_{R^3} 2(f-u)(-\triangle u)\delta(\varphi)|\nabla\varphi| d\vec{x} \\
&= \int_{R^3} p|P_{\nabla\varphi}\nabla u|^{p-2}P_{\nabla\varphi}\nabla u \cdot P_{\nabla\varphi}\nabla(\triangle u)\delta(\varphi)|\nabla\varphi| d\vec{x} \\
&\quad - \lambda_D \int_{R^3} (f-u) \triangle u\delta(\varphi)|\nabla\varphi| d\vec{x} \\
&= \int_{R^3} p|P_{\nabla\varphi}\nabla u|^{p-2}P_{\nabla\varphi}\nabla u \cdot (\nabla(\triangle u))\delta(\varphi)|\nabla\varphi| d\vec{x} \\
&\quad - \lambda_D \int_{R^3} (f-u) \triangle u\delta(\varphi)|\nabla\varphi| d\vec{x} \\
&= -\int_{R^3} \nabla\cdot(p|P_{\nabla\varphi}\nabla u|^{p-2}P_{\nabla\varphi}\nabla u\delta(\varphi)|\nabla\varphi|) \triangle u d\vec{x} \\
&\quad - \lambda_D \int_{R^3} (f-u) \triangle u\delta(\varphi)|\nabla\varphi| d\vec{x} \\
&= -\int_{R^3} (\nabla\cdot(p|P_{\nabla\varphi}\nabla u|^{p-2}P_{\nabla\varphi}\nabla u|\nabla\varphi|)\delta(\varphi) \\
&\quad + (p|P_{\nabla\varphi}\nabla u|^{p-2}P_{\nabla\varphi}\nabla u|\nabla\varphi|)\cdot(\delta'(\varphi)\nabla\varphi)) \triangle u d\vec{x} \\
&\quad - \lambda_D \int_{R^3} (f-u) \triangle u\delta(\varphi)|\nabla\varphi| d\vec{x} \\
&= -\int_{R^3} (\nabla\cdot(p|P_{\nabla\varphi}\nabla u|^{p-2}P_{\nabla\varphi}\nabla u|\nabla\varphi|) \\
&\quad + \lambda_D(f-u)|\nabla\varphi|)\delta(\varphi) \triangle u d\vec{x} \\
&= -\int_S \frac{1}{|\nabla\varphi|}(\nabla\cdot(p|P_{\nabla\varphi}\nabla u|^{p-2}P_{\nabla\varphi}\nabla u|\nabla\varphi|) \\
&\quad + \lambda_D(f-u)|\nabla\varphi|) \triangle u dS \\
&= -\int_S (\frac{1}{|\nabla\varphi|}\nabla\cdot(p|P_{\nabla\varphi}\nabla u|^{p-2}P_{\nabla\varphi}\nabla u|\nabla\varphi|) \\
&\quad + \lambda_D(f-u)) \triangle u dS
\end{aligned}$$

Because the energy is minimal, that is, $\triangle E \equiv 0$ for any $\triangle u$, so

$$\frac{1}{|\nabla\varphi|}\nabla\cdot(p|P_{\nabla\varphi}\nabla u|^{p-2}P_{\nabla\varphi}\nabla u|\nabla\varphi|) + \lambda_D(f-u) = 0$$

This is the Euler-Lagrange equation corresponding to energy functional E.

(b)Under the given condition, this is straightforward via differentiating E. ■

The condition of energy minimizing is given for general case in Theorem 2(a). When numerical computing, we convert the Euler-Lagrange equation to a time developing equation as showed in Theorem 2(b). In this paper, we study a special and important case of $p = 1$(Intrinsic Total Variation energy). The corresponding Euler-Lagrange equation is an anisotropic diffusion equation:

$$\frac{1}{|\nabla\varphi|}\nabla\cdot\Big(\frac{P_{\nabla\varphi}\nabla u}{|P_{\nabla\varphi}\nabla u|}|\nabla\varphi|\Big)+\lambda_D(f-u)=0(u_t) \quad (17)$$

Numerical method in detail is given in next section.

3.4 Numerical Method

In this section numerical scheme for equation (16) is given. Although our Euler-Lagrange equation is obtained on S, we still should solve it in a band around S for numerical computing of ∇u. Therefore, at first, we extrapolate the image data given on S to a band around S such that the extrapolated data keep constant along the normal directions of the level sets of φ as mentioned above. Our model is intrinsic to the surface S since we project the gradient of data to the tangent plane of the level sets of φ. A grid cell in the solving band is showed in Fig. 4.

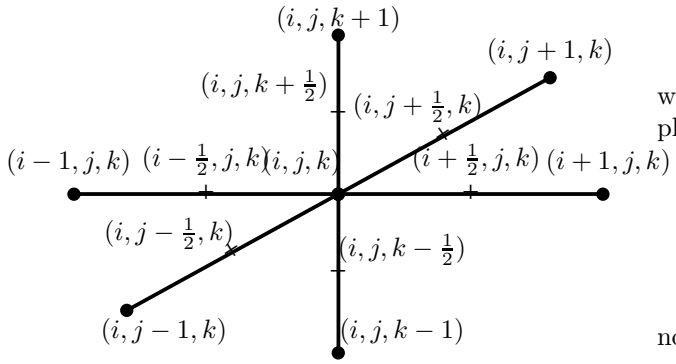

Figure 4: Grid cell

In [20] a discrete method of first forward then backward difference scheme is proposed to treat derivative term of order 2. In fact this method is equivalent with the straightforward central difference scheme for linear operator ($p = 2$) but not with any nonlinear cases ($p \neq 2$) in equation (16), such as our Intrinsic Total Variation model. So another discrete scheme is given in the follows.

Let $V = (V^1, V^2, V^3) = p|P_{\nabla\varphi}\nabla u|^{p-2}P_{\nabla\varphi}\nabla u|\nabla\varphi|$, we have

$$\begin{aligned}&(\nabla\cdot(p|P_{\nabla\varphi}\nabla u|^{p-2}P_{\nabla\varphi}\nabla u|\nabla\varphi|))_{(i,j,k)}\\ =&(V^1_x)_{(i,j,k)}+(V^2_y)_{(i,j,k)}+(V^3_z)_{(i,j,k)}\\ =&\frac{V^1_{(i+\frac{1}{2},j,k)}-V^1_{(i-\frac{1}{2},j,k)}}{\triangle x}+\frac{V^2_{(i,j+\frac{1}{2},k)}-V^2_{(i,j-\frac{1}{2},k)}}{\triangle y}\\ &+\frac{V^3_{(i,j,k+\frac{1}{2})}-V^3_{(i,j,k-\frac{1}{2})}}{\triangle z}\end{aligned}$$

Taking $V^1 = p|P_{\nabla\varphi}\nabla u|^{p-2}(u_x - \frac{\nabla u\cdot\nabla\varphi}{|\nabla\varphi|^2}\varphi_x)|\nabla\varphi|$ for example, we introduce our difference scheme at semi-grid points.

At first, we compute the derivatives of φ. Because φ does not change as time grows up, only once computation of these derivatives is needed. We average the derivatives at grid points to get the derivative at semi-grid points. For example, at semi-grid point $(i+\frac{1}{2},j,k)$,

$$\begin{aligned}(\varphi_x)_{(i+\frac{1}{2},j,k)}&=((\varphi_x)_{(i,j,k)}+(\varphi_x)_{(i+1,j,k)})/2\\ (\varphi_y)_{(i+\frac{1}{2},j,k)}&=((\varphi_y)_{(i,j,k)}+(\varphi_y)_{(i+1,j,k)})/2\\ (\varphi_z)_{(i+\frac{1}{2},j,k)}&=((\varphi_z)_{(i,j,k)}+(\varphi_z)_{(i+1,j,k)})/2\end{aligned}$$

while at grid points central difference scheme is applied:

$$\begin{aligned}(\varphi_x)_{i,j,k}&=(\varphi_{(i+1,j,k)}-\varphi_{(i-1,j,k)})/(2\triangle x)\\ (\varphi_y)_{i,j,k}&=(\varphi_{(i,j+1,k)}-\varphi_{(i,j-1,k)})/(2\triangle y)\\ (\varphi_z)_{i,j,k}&=(\varphi_{(i,j,k+1)}-\varphi_{(i,j,k-1)})/(2\triangle z)\end{aligned}$$

The discrete scheme for the space derivatives of u is not simple. We adopt the so-called Minmod function proposed by S. Osher, *et al.* Again we take the semi-grid point $(i+\frac{1}{2},j,k)$ as an example (Fig. 4),

$$\begin{aligned}(u_x)_{(i+\frac{1}{2},j,k)}&=(u_{(i+1,j,k)}-u_{(i,j,k)})/\triangle x\\ (u_y)_{(i+\frac{1}{2},j,k)}&=\mathrm{Minmod}\Big(\frac{u_{(i,j+1,k)}-u_{(i,j-1,k)}}{2\triangle y},\end{aligned}$$

$$\frac{u_{(i+1,j+1,k)} - u_{(i+1,j-1,k)}}{2 \triangle y}\Big)$$

$$(u_z)_{(i+\frac{1}{2},j,k)} = \text{Minmod}\Big(\frac{u_{(i,j,k+1)} - u_{(i,j,k-1)}}{2 \triangle z},$$

$$\frac{u_{(i+1,j,k+1)} - u_{(i+1,j,k-1)}}{2 \triangle z}\Big)$$

where

$$\text{Minmod}(a,b) = \frac{\text{sign}(a) + \text{sign}(b)}{2} \min(|a|, |b|)$$

here $\text{sign}(\cdot)$ is the sign function.

For $(\lambda_D(f-u))_{(i,j,k)}$ we take the value of the grid point straightly. Forward difference scheme is applied to u_t. Integrating these discrete schemes, the numerical scheme of equation (16) is obtained. Numerical schemes with high order accuracy (for example TVD-RK with WENO scheme) can be constructed, but much extra algorithm complexity may also be produced. Experiments in the next section show our numerical method works efficiently and generates satisfying results.

4 Algorithm Steps and Experiment Results

Based on the energy functional and numerical method, in this section, we describe our inpainting algorithm of images on implicit surfaces in detail. Then some experiment examples are presented.

Assume we have an implicit surface S as the zero level set of φ. f is an observed image on S and the information on $D \subset S$ is missing or distorted. Our inpainting algorithm is:

a Extrapolate the image data f to a band according to equation (10);

b Extrapolate the inpainting mask 1_D to the same band according the equation (10) (controlling the resolution time);

c For any grid points in the extrapolated band, if the corresponding extrapolated inpainting mask is greater than 0.5, then mark it to be 1; else mark it to be 0;

d Determine a solving band within the band obtained in (a) and (b) according to the data extrapolating theorem 1. Then solve equation (16) using f as the initial condition.

Note that step (c) is necessary. Because of numeric errors, the extrapolated inpainting mask at some points in the band may not accurately equal to 0 or 1. The parameter λ in our inpainting model is just for domain $S \backslash D$ and should not affect the information in domain D. So an acurrate inpainting mask is needed and (c) is necessary.

Several examples are presented to finish the section. Because of the use of straightforward Cartesian numerics, the overall algorithmic complexity is reduced and the implementation is simplified. In our experiments, the functions presenting surfaces are all signed distance functions, that is, $|\nabla\varphi| \equiv 1$. We made the extrapolating equation to run a period of time $t_e = 20 \times h$ in step (a) and (b), where h is the grid scale. Then we can choose a band $B = \{(x,y,z) : -t_s \leq \varphi(x,y,z) \leq t_s, t_s \leq t_e\}$ for our inpainting model in step (d). In our experiments we chose $t_s = 5 \times h$ and $\lambda = 20000$. We studied a special and important case of $p = 1$(Intrinsic Total Variation energy) as mentioned before in our experiments.

The surface in Fig. 5 is a sphere. We defined an image of a triangle on it. In Fig. 5(a) the image was distorted. Fig. 5(b) is the inpainted result. In this example, our inpainting algorithm not only repaired the distorted image but also denoised it. The volume used contains $148 \times 148 \times 148$ voxels.

A more complex example of Lena on a bottle is shown in Fig. 6. The distorted image is shown in Fig. 6(a). There are many scratches on it. Furthermore, some scratches crossed the edges of the image. By our inpainting model, the image is inpainted perfectly not only in the smooth area but also at the image edges, as shown in Fig. 6(b). This is the very advantage of the Intrinsic Total Variation energy model. The volume used contains $216 \times 130 \times 125$ voxels.

Fig. 7 shows an example of image on a general surface. There is a horse and an image of Chinese character "刀" is defined on it. Suppose for various reasons the character image was distorted where a

few scratches appeared. Furthermore, some scratches crossed the edge of the character image. Fig. 7(b) is the inpainting result. Here we see the advantage of the Intrinsic Total Variation energy model again. Our inpainting model is robust for distortion at smooth area and discontinues area (edges) of images. The volume used contains $220 \times 187 \times 112$ voxels.

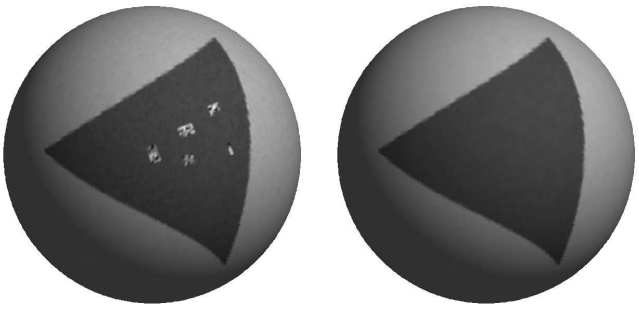

a b

Figure 5: A triangle on sphere

a b

Figure 6: Lena on a bottle

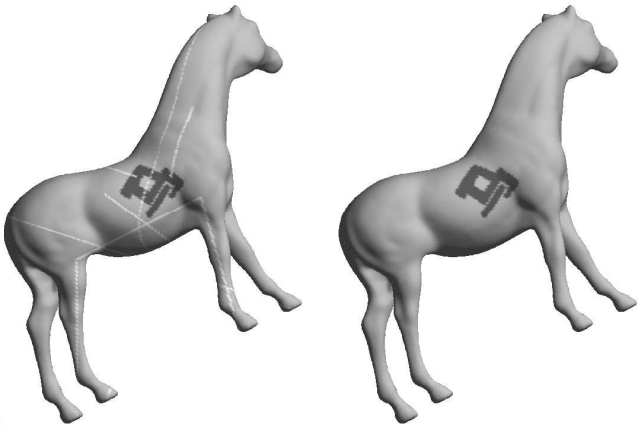

a b

Figure 7: A Chinese character on a horse

5 Conclusion and Future Work

In this paper we generalized an inpainting algorithm of planar images to the case of images on general implicit surfaces via generalizing energy functionals. Especially we studied an important inpainting model based on Intrinsic Total Variation energy model. In addition, we obtained a theorem about data extrapolating needed in numerical computing. According to this theorem, users can choose a valid and correct band to solve their inpainting equation.

It should be pointed out that the distorted domain D is supposed to be known in our algorithm. In fact the detection of D is a problem. We suggest two ways for solving it. The first one is an automatically detection method based on learning theory and artificial intelligence. The second one is based on man-machine conversation. In the latter the distorted domain is chosen by users. The geometry information of surfaces will be used for correctness.

Another future work is to inpaint color images (vector valued images) on implicit surfaces. For color images, channel by channel method may be used or other methods based on seemly energy functionals of vector valued data.

Acknowledgments

The authors are support by the Outstanding Youth Grant of NSF of China (No. 60225002), NSF of China (10201030 and 60473132), a National Key Basic Research Project of China (2004CB318000), the TRAPOYT in Higher Education Institute of MOE of China, and SRF for ROCS, SEM. We thank Xuchuan Fan for his help on signed distance function and Yan Xu for her help on the numerical methods of Hamilton-Jacobi equation.

References

[1] P. Perona and J. Malik. Scale-space and edge detection using anisotropic diffusion. IEEE Trans. Pattern Anal. Machine Intell., 12(7), 629–639, 1990.

[2] L. Rudin, S. Osher, and E. Fatemi. Nonlinear total variation based noise removal algorithms. Physica D, 60, 259–268, 1992.

[3] T.F. Chan, S. Osher, and J. Shen. The digital TV filter and nonlinear denoising. IEEE Trans. and Image Process, 10(2), 2001.

[4] T.F. Chan and P. Mulet. Iterative Methods for Total Variation Image Restoration. Iterative Methods in Scientific Computing, Hong Kong, 1995.

[5] C.R. Vogel, M.E. Oman. Iterative Methods for Total Variation Denoising. SIAM J. Sci. Comput., 17(1), 227-238, 1996.

[6] C.R. Vogel, and M.E. Oman. Fast, robust total variation-based reconstruction of noisy, blurred images. IEEE Trans. Image Processing, 7, 813-824, 1998.

[7] T.F. Chan, S.H. Kang and J. Shen. Total Variation Denoising and Enhancement of Color Images Based on the CB and HSV Color Models. Journal of Visual Communication and Image Representation, 12, 422–435, 2001.

[8] M. Bertalmio and G. Sapiro, V. Caselles and C. Ballester. Image inpainting. Compuer Graphics, SIGGRAPH 2000, 417–424, 2000.

[9] T.F. Chan and J. Shen. Mathematical models for local nontexture inpaintings. SIAM J. Appl. Math. 62(3), 1019–1043, 2001.

[10] T.F. Chan and J. Shen. Non-texture inpainting by curvature-driven diffusions(CDD). J. Visual Comm. Image Rep., 12(4), 436–449, 2001.

[11] T.F. Chan, S.H. Kang and J. Shen. Euler's elastica and curvature based inpaintings. SIAM J. Appl. Math., 63(2), 564–592, 2002.

[12] S. H. Kang, T. F. Chan, and S. Soatto. Landmark based Inpainting from Multiple Views. UCLA Math CAM 02-11, 2002.

[13] T.F. Chan, J. Shen, and L. Vese. Variational PDE models in image processing. Notice of Amer. Math. Soc., 50, 14–26, 2003.

[14] M.M. Oliveira, B. Bowen, R. McKenna, Y.S. Chang. Fast digital image inpainting. Proceedings of the International Conference on Visualization, Imaging and Image Processing (VIIP2001), Marbella, Spain. 261–266, 2001.

[15] S. Esedoglu and J. Shen. Digital inpainting based on the Mumford-Shah-Euler image model. European J. Appl. Math., 13, 353–370, 2002.

[16] M. Bertalmio, A.L. Bertozzi, and G. Sapiro. Navier-Stokes, fluid dynamics, and image and video inpainting. Proc. IEEE Computer Vision and Pattern Recognition (CVPR), Hawaii, 2001.

[17] J. Shen. Inpainting and the Fundamental Problem of Image Processing. SIAM News, 36(2), 2003.

[18] J. Shen. Bayesian Video Dejittering By BV Image Model. SIAM J. Appl. Math., 64(5), 1691–1708, 2004.

[19] T.F. Chan, L.A. Vese. A level set algorithm for minimizing the Mumford-Shah functional in image processing. IEEE/Comput. Soc. Proc. of the

1st IEEE Workshop on Variational and Level Set Methods in Computer Vision, 161–168, 2001.

[20] M. Bertalmio, L.T. Cheng, S. Osher, G. Sapiro. Variational Problems and Partial Differential Equations on Implicit Surfaces. J. Comput. Phys., 174(2), 759–780, 2001.

[21] B. Tang, G. Sapiro, V.Caselles. Diffusion of General Data on Non-Flat Manifolds via Harmonic Maps Theory:The Direction Diffusion Case. International Journal of Computer Vision 36(2), 149–161, 2000.

[22] S. Chen, B. Merriman, S. Osher, and P. Smereka. A simple level set method for solving Stefan problems. J. Comput. Phys., 135, 8–29, 1997.